Earth Planets Space, **65**, 1477–1489, 2013

Volcano inflation prior to an eruption: Numerical simulations based on a 1-D magma flow model in an open conduit

Ryohei Kawaguchi, Takeshi Nishimura, and Haruo Sato

Department of Geophysics, Graduate School of Science, Tohoku University, Aramaki-aza Aoba 6-3, Aoba-ku, Sendai, Miyagi 980-8578, Japan

(Received July 30, 2012; Revised March 6, 2013; Accepted May 3, 2013; Online published December 6, 2013)

We numerically simulate volcanic inflation caused by magma ascent in a shallow conduit at volcanoes which repeatedly erupt, in order to understand the effect of volatile behavior on magma from geodetic data. Considering magma in which the relative velocities between melt and gas bubbles are negligible, we model magma flow in a one-dimensional open conduit with diffusive gas bubble growth. We calculate the ground displacements and tilts caused by spatio-temporal changes of magma pressure in the conduit. Our simulations show that magma without volatiles causes decelerated changes in volcanic inflation. Magma with gas bubble growth inflates the volcano with a constant, or accelerated, rate. Temporal changes of volcanic deformation are also affected by the magma pressure at the bottom of the conduit. When the pressure is small, the displacements and tilts increase in proportion to the 1.5th power of time. This time rate is similar to that predicted from a basic gas bubble growth model. When the pressure equals the lithostatic pressure, the effects of gas bubble growth relatively decrease and the displacements and tilts increase linearly with time.

Key words: Volcano inflation, 1-d conduit flow model, bubble growth, temporal change.

1. Introduction

Volatile behavior in magma plays an important role in eruption styles and intensities. To understand the physical processes in magma that control magma ascent and eruption styles, many studies have been conducted on the basis of laboratory experiments, numerical calculations and theoretical considerations. Theoretical and numerical models have examined bubble growth processes at micro scales, and clarified that the bubble growth rate mainly depends upon the amount of volatiles saturated in the melt and the physical properties of the melt such as the viscosity and diffusion coefficients of the volatiles in the melt (e.g., Sparks, 1978; Proussevitch *et al*., 1993; Proussevitch and Sahagian, 1996; Lensky *et al*., 2004). Laboratory experiments have clarified the volatile behavior and the physical properties of magma (e.g., Lyakhovsky *et al*., 1996; Okumura *et al*., 2008). For example, Lyakhovsky *et al*. (1996) performed a gas bubble growth experiment under high pressure and high temperature conditions, and measured the bubble radius and the number density of bubbles for a rhyolitic hydrated melt. Their experimental results are well explained by the theoretical bubble growth model presented by Proussevitch *et al*. (1993). They also showed that the bubble radius growth rate is proportional to the square root of time when the bubble growth process is subjected to the diffusion of volatiles.

Numerical simulations have investigated the macro-scale magma ascent processes in magmatic conduits to elucidate the mechanism of volcanic eruptions. For sustained Plinian type eruptions, steady-state magma flow models have revealed the importance of magma properties and conduit shape on the dynamics of magma flow and volcanic eruption styles (e.g., Wilson *et al*., 1980; Woods and Koyaguchi, 1994; Yoshida and Koyaguchi, 1999; De Michieli Vitturi *et al*., 2008). Non-sustained Vulcanian eruptions have also been studied by using time-dependent magma flow models (e.g., Barmin *et al*., 2002; Melnik and Sparks, 2002; Costa *et al*., 2007; Mason *et al*., 2006; Ida, 2007; Nakanishi and Koyaguchi, 2008; Anderson and Segall, 2011). Melnik and Sparks (2002) and Mason *et al*. (2006) showed that the substantivity of explosive eruptions is significantly affected by the volatile behavior in magma: when volatiles can diffuse fast enough in the magma, the eruption becomes a sustained Plinian eruption, while magma with a slow diffusion of volatiles turns an eruption into a short-lived Vulcanian explosion.

In addition to these laboratory and theoretical studies, analyses of geophysical data obtained at active volcanoes have been intensively conducted to capture 'in situ' magmatic motion. For example, geodetic data analyses are useful for determining the locations and sizes of volcanic pressure sources by applying pressure source models (Mogi, 1958; Okada, 1985; Davis, 1986). Recent observations conducted at active craters have succeeded in detecting tiny inflation and deflation signals associated with small Vulcanian or Strombolian explosions with high resolution. For example, at the Stromboli volcano, small inflations that accelerate with time are observed for repetitive explosions (Ripepe and Harris, 2008). At the Semeru volcano in Indonesia, accelerating inflations are also observed 200–300

doi:10.5047/eps.2013.05.005

s before small Vulcanian eruptions, while gas burst events follow the inflations for about 20 s with a constant rate (Nishi *et al.*, 2007; Iguchi *et al.*, 2008; Nishimura *et al.*, 2012). Inflations prior to small Vulcanian eruptions are also observed at the Suwanosejima volcano, Japan (Iguchi *et al.*, 2008). These inflations are thought to result from pressurization processes associated with magma ascent and/or gas flow in the shallow conduit.

It is quite important to quantitatively relate the geodetic data that capture macro-scale magma behavior with micro-scale phenomena in the magma to elucidate the magma dynamics and eruption mechanisms. Simple models, including the interaction between gas bubbles in the magma and the surrounding elastic rock, are presented by, for example, Nishimura (2004) and Shimomura *et al.* (2006). These results are used to understand the inflation processes, or oscillating crack motions, detected by geodetic and seismic observations (Chouet *et al.*, 2006; Voight *et al.*, 2006). Relationships between geodetic data and magma ascent, including macro-scale phenomena, have also been theoretically examined. Nishimura (2006) showed that magma ascent without out-gassing causes accelerated volcanic inflation that may lead to explosive eruptions. Magma ascent with out-gassing gradually inflates the volcano and causes non-explosive eruptions. His results suggest that geodetic measurements are useful in capturing micro-scale phenomena in magma that may control eruption styles.

The present study focuses on repetitive eruptions, such as Vulcanian type, to understand the relationship between micro-scale phenomena in magma and inflation processes prior to eruptions. These eruptions occur over a relatively short time interval, and the conduit system is considered to be open so that magma ascent is not significantly affected by the surrounding rocks. Nishimura (2009) recently studied volcanic inflation associated with such repetitive eruptions, and separately examined the inflations for three basic processes of magma ascent: Poiseuille flow, gas bubble growth due to diffusive gas flow, and rising gas bubble. However, the real magma ascent process in a volcanic conduit is a composite phenomenon consisting of these basic processes. Hence, it is necessary to examine magma flow that includes the expansion of gas phases in an open conduit. At a shallow depth in the conduit, there are two primary mechanisms that can expand the volume of gas phases: diffusive flow of water molecules from saturated melt to gas bubbles, and pressure differences between the gas and the surrounding melt. The present study examines magma flow mainly including the former mechanism, which may occur at volcanoes characterized by a viscous magma (e.g. andesitic magma) in which the relative velocity between the gas bubbles and the melt is taken to be negligibly small. We formulate the basic equations of two-phase magma flow to represent the magma ascent, including the Poiseuille flow and diffusive bubble growth processes, to study the temporal changes of volcanic inflation prior to eruptions. Since the melt and gas bubbles are supposed to ascend at the same speed, our model does not target the eruptions of low-viscous magma. First, we present a two-phase magma flow model in a one-dimensional open conduit using the basic equations of magma flow. Subsequently, we calculate temporal changes of volcanic deformation using the spatio-temporal distribution of magma pressure in the conduit that is calculated by the magma flow model. Simulating the magma ascent for different parameters of magma properties related to the bubble growth process, we discuss the relationship between the magma properties in the conduit to volcanic deformation.

2. Model

2.1 Magma ascent process in repetitive eruptions

Vulcanian-type eruptions that occur every few to tens of minutes are considered to be generated from repetitive magma ascent in open conduits. Hence, the opening and closing of the conduit is not taken into account in the modeling of magma ascent processes. Also, as seismic sources associated with such eruptions are estimated to originate at shallow depths below the active crater (e.g. a few hundred meters for the Suwanose-jima volcano, Tameguri *et al.* (2004)), we assume a relatively simple conduit system that vertically extends downward from the active crater. A schematic illustration of the magma ascent process and the magma pressure distribution in an open conduit is shown in Fig. 1. Just before an eruption, the conduit is almost completely filled with magma, and the magma pressure linearly increases with depth. When an eruption occurs, the magma filling the upper part of the conduit is effused in a short time. As a result, magma residing in the shallow part of the conduit is subjected to rapid depressurization. Magma pressure at the deeper portion of the conduit does not change when the magma viscosity is high, and/or the conduit is narrow (Nishimura, 2009). Just after the eruption, the solubility of volatiles in the melt decreases so that the volatiles supersaturate in the melt. Gas bubbles contained in the magma cannot expand quickly because of viscous resistance from the surrounding melt. As time proceeds, the gas bubbles slowly grow as a result of the pressure difference built up between the gas bubbles and the melt and also by the mass flux of volatiles from the supersaturated melt. The magma moves upward due to the volume expansion caused by the gas bubble growth and a pressure gradient builds up in the conduit. As the magma ascends in the conduit, the pressure acting on the conduit wall increases and the volcano inflates. When the magma reaches the top of the conduit, or satisfies a triggering condition of eruption, a new eruption starts. In the preset study, we model the magma ascent process from just after an eruption to just before an eruption.

Magma motions in a conduit have often been studied by one-dimensional non-steady two-phase magma flow models (Melnik and Sparks, 2002; Mason *et al.*, 2006; Ida, 2007). These models suppose that diffusive gas flow is the dominant process that expands the volume of the gas phase, and that the relative velocities between the gas phase and the melt is negligibly small. The present study also assumes these conditions. For instance, the gas bubbles need to be characterized with a radius of less than about 10^{-1} m, for a magma with a viscosity of 10^4–10^5 Pa s, because relative velocities between the gas bubbles and the melt are estimated to be less than 10^{-5}–10^{-4} m/s from Stokes' law. We further neglect nucleation and the coalescence of gas bubbles, and out-gassing processes from the magma into the

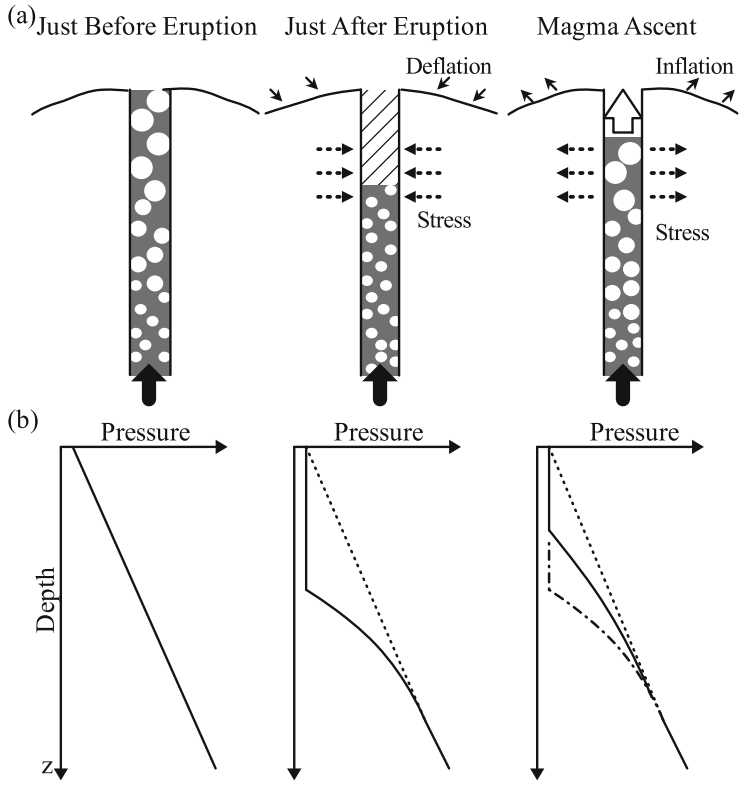

Fig. 1. (a) Schematic illustration of the magma ascent process in an open conduit. (b) Spatial distribution of magma pressure in the conduit. Solid lines show the magma pressure at each stage. Dotted lines show the magma pressure just before an eruption. Chained line shows the magma pressure just after an eruption.

surrounding medium, in our model. These are important basic processes for magma dynamics at a shallow depth; however, this paper is a first attempt to formulate relationships between magma flow models and ground deformation. Hence, we do not take into account these processes in the present study.

We simulate an open conduit and changes in the conduit radius caused by magma pressure. In the shallow part of the conduit (< 1 km), magma pressure variations are predicted to be less than tens of MPa from the lithostatic pressure. Assuming a rigidity of surrounding rocks of 1–10 GPa at a depth of 1 km, we estimate the changes of the circular conduit radius to be 0.025–0.25%. Even when the conduit shape is elliptical, with an aspect ratio of 10, the radius change is 2.5%. These values are negligibly small compared with changes in the magma flow within the conduit, so that we may reasonably assume a conduit with a constant radius.

2.2 Governing equations of magma flow in an open conduit

To express the magma ascent process, we use the equations of mass conservation, motion and state of gas and melt phases. Notations used in the equations are summarized in Table 1. The equations of mass conservation for the two-phase magma and exsolved volatile in the gas bubbles are written as:

$$\frac{\partial \rho}{\partial t} = -\frac{\partial}{\partial z}(\rho v), \tag{1}$$

Table 1. Notations used in this study.

ρ	Bulk magma density
ρ_l	Melt density
ρ_e	Ex-solved volatile density
p	Melt pressure
p_g	Gas pressure
η_f	Melt viscosity
v	Magma ascent velocity
ψ	Void ratio
a	Conduit radius
g	Gravity acceleration
J	Mass flux of volatile
B	Universal gas constant
T	Magma temperature
K_l	Bulk modulus of melt
R_g	Bubble radius
S	Cell radius
c	Volatile concentration
n	Bubble number density
D	Diffusivity of volatile in melt
t	Time
z	Vertical coordinate

$$\frac{\partial \rho_e}{\partial t} = -\frac{\partial}{\partial z}(\rho_e v) + J, \tag{2}$$

where ρ is the density of two-phase magma, ρ_e is the density of gas in the bubbles, J is the mass flux of volatile

from supersaturated melt to gas bubbles per unit volume of magma, v is the magma ascent velocity, t is the time measured from the eruption, and z is the vertical coordinate with $z = 0$ corresponding to the ground surface. The vertical coordinate is positive in the downward direction. Since gas and melt phases are assumed to have the same ascent velocity, the equation of motion of two-phase magma is expressed by that of a one-phase viscous fluid. Inertial terms in the equation of motion are assumed to be negligibly small because of the high viscosity of magma in our model, so we obtain:

$$v = -\frac{a^2}{8\eta_f}\left(\frac{\partial p}{\partial z} + \rho g\right), \tag{3}$$

where a is the conduit radius, η_f is the melt viscosity, p is the melt pressure, and g is the gravitational acceleration. The density of two-phase magma is expressed by the densities of the gas and melt phases and the gas volume fraction ψ:

$$\rho = (1 - \psi)\rho_l + \rho_e, \tag{4}$$

where ρ_l is the density of the melt. Assuming that the gas phase in the bubbles is represented as a perfect gas and the melt is compressible viscous fluid, we obtain the equations of state of the gas and liquid melt phases:

$$\rho_l = \rho_r\left(1 + \frac{p - p_r}{K_l}\right), \quad \rho_e = \psi\frac{p_g}{BT}, \tag{5}$$

where p_r and ρ_r are the pressure and density of the melt at a reference depth (we may assume the bottom of the conduit), respectively, p_g is the pressure of the gas phase in the gas bubbles, K_l is the bulk modulus of the melt, B is the universal gas constant divided by the molecular weight of a gas molecule, and T is the absolute temperature of the magma. Here, we suppose a constant temperature of the magma independent of depth and time.

2.3 Governing equations of gas bubble growth process in magma

We formulate the gas bubble growth process in magma by applying the cell model proposed by Arefmanesh and Advani (1991), and Proussevitch *et al.* (1993). This model supposes that magma is composed of numerous elemental spherical cells which have one gas bubble at the center of each cell (Fig. 2). Therefore, the numerous gas bubble growth processes are represented by the motion of one elementary cell. The momentum equation of a Newtonian fluid that surrounds a spherical gas bubble can be written as (Scriven, 1959; Melnik and Sparks, 2002):

$$\frac{\partial R_g}{\partial t} = -v\frac{\partial R_g}{\partial z} + \frac{R_g}{4\eta_f}(p_g - p)\left(\frac{S^3}{S^3 - R_g^3}\right), \tag{6}$$

where R_g is the gas bubble radius and S is the elementary cell radius. In this equation, the surface tension term is neglected, because the effect of surface tension is small for gas bubbles at a shallow depth where the gas bubble radius is considered to be large ($>10^{-5}$ m).

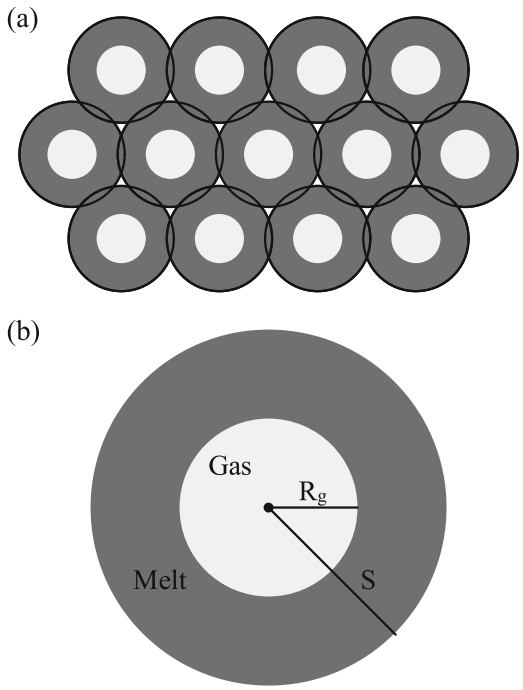

Fig. 2. Schematic illustration of (a) cell model and (b) elementary cell. Magma is represented by many elementary cells. Each cell includes a single gas bubble at its center. R and S are the radius of the elementary cell and that of the gas bubble, respectively.

The diffusive flow of the volatiles dissolved within the melt into the gas bubble is governed by the diffusion equation:

$$\frac{\mathrm{D}c}{\mathrm{D}t} = D\frac{1}{r^2}\frac{\partial}{\partial r}\left(r^2\frac{\partial c}{\partial r}\right), \tag{7}$$

where c is the concentration of volatiles in the melt, D is the diffusive coefficient of the volatiles in the melt, $\mathrm{D}/\mathrm{D}t$ is the total derivative, and r is the radial coordinate. The mass change of volatiles in the gas bubble is related to the diffusive mass flux of volatiles into the gas bubble, which depends on the concentration gradient of volatiles on the bubble melt interface:

$$\frac{\mathrm{d}}{\mathrm{d}t}\left(\frac{4}{3}\pi {R_g}^3\rho_g\right) = 4\pi {R_g}^2 D\rho_l\left(\frac{\partial c}{\partial r}\right)_{r=R_g}. \tag{8}$$

The total mass flux of volatile J is expressed by using the number density of the gas bubbles:

$$J = 4\pi n {R_g}^2 D\rho_l\left(\frac{\partial c}{\partial r}\right)_{r=R_g}, \tag{9}$$

where n is the number density of the gas bubbles.

Here, we consider that diffusive mass transfer primarily drives the gas bubble growth process, where the Peclet number Pe, which is the ratio of the characteristic time for diffusion of volatiles to viscous deformation, is small. In this case, the unsteady term in the diffusion equation (Eq. (7)) can be neglected, because diffusion is fast enough to establish a steady-state concentration distribution of volatiles in

the melt. Thus, the diffusion equation can be rewritten as:

$$D\frac{1}{r^2}\frac{\partial}{\partial r}\left(r^2\frac{\partial c}{\partial r}\right)=0\,. \tag{10}$$

This approximation enables us to obtain an analytical solution of volatile concentration distribution in the melt, which is expressed as (Lyakhovsky *et al.*, 1996):

$$c(r)=C_1-C_2\frac{1}{r}, \tag{11}$$

where C_1 and C_2 are integration constants. Using the mass conservation law and Henry's law, $c(R_g)=\left(K_h p_g\right)^{1/2}$, where K_h is Henry's constant, we can determine C_1 and C_2 as follows (Mason *et al.*, 2006):

$$C_1=c(R_g)+\frac{C_2}{R_g}\,, \tag{12a}$$

$$C_2=\frac{2R_g\left(c_0S_0^3-\left(S^3-{R_g}^3\right)c\left(R_g\right)-\frac{\rho_g}{\rho_l}{R_g}^3\right)}{2S^3+{R_g}^3-3S^2R_g}, \tag{12b}$$

where c_0 is the volatile concentration in the melt when the gas bubble radius is negligibly small. By substituting Eqs. (11)–(12b) into Eq. (9), the mass flux of volatiles into the melt is rewritten as:

$$\begin{aligned}J&=4\pi nD\rho_l C_2\\&=4\pi nD\rho_l\frac{2R_g\left(c_0S_0^3-\left(S^3-{R_g}^3\right)c\left(R_g\right)-\frac{\rho_g}{\rho_l}{R_g}^3\right)}{2S^3+{R_g}^3-3S^2R_g}.\end{aligned} \tag{13}$$

To connect the equations of the magma flow in the conduit and the gas bubble growth process described above, we further introduce the equations relating the gas bubble radius R_g, the cell radius S, the number density of the gas bubbles n, and the gas volume fraction ψ:

$$\frac{4\pi}{3}n{R_g}^3=\psi\,,\ \frac{4\pi}{3}nS^3=1\,,\ \frac{4\pi}{3}n_*S_*^3=1, \tag{14}$$

where the subscript * represents the value when the gas bubble radius is small enough to neglect its volume at the deeper portion of the conduit. By using the above relationships, the bubble number density is related to the void ratio:

$$n=(1-\psi)\,n_*. \tag{15}$$

The bubble number density per unit volume of magma changes with the expansion of the magma cell due to depressurization. In Eqs. (14) and (15), we suppose that the melt volume is constant. This is because pressure variations are less than tens of MPa in our simulation range, while the bulk modulus of the melt is on the order of tens of GPa. Hence, the melt volume change is negligibly small ($< 0.1\%$). Although we assume a compressible melt in Eq. (5), the relationships in Eq. (14) can be useful. Substituting Eq. (14) into Eqs. (6) and (13), we obtain:

$$\frac{\partial\psi}{\partial t}=-v\frac{\partial\psi}{\partial z}+\frac{3\psi}{4\eta_f}(p_g-p)\left(\frac{1}{1-\psi}\right), \tag{16}$$

$$\begin{aligned}J=&\,4(6\pi^2)^{\frac{1}{3}}n_*^{\frac{2}{3}}D\rho_l\\&\cdot\frac{\left(\psi^3+\psi-2\psi^2\right)^{\frac{1}{3}}\left((1-\psi)(c_0-c(R_g))-\psi\frac{\rho_e}{\rho_l}\right)}{2+\psi-3\psi^{\frac{1}{3}}}.\end{aligned} \tag{17}$$

The magma ascent process, including the gas bubble growth process, in the cylindrical conduit is calculated using the above two equations (Eqs. (16) and (17)) and the governing equations of magma flow (Eqs. (1)–(5)) as a function of depth z and time t.

2.4 Initial and boundary conditions

Pressure waves, caused by a withdrawal of magma at the top of the conduit due to an eruption, do not reach the deeper portion of the conduit when the magma viscosity is high and the bulk modulus of the magma is small (Nishimura, 2009). Hence, we suppose that the pressure at the bottom of the conduit p_0 is constant. The pressure above the magma head depth in the open conduit is also set to be constant p_h. The melt pressure linearly increases with depth.

We also need to set the initial value of the volatile concentration in the melt (c_0), the magma head depth in the conduit (z_{m0}), and the initial pressure difference between the gas bubbles and the melt (Δp). Note that the volatile concentration, c_0, is defined for a magma without gas bubbles and that the initial volatile concentration in the melt changes with depth, due to the pressure dependence of the solubility of volatiles in the melt. The initial gas pressure ($p_{g0}(z)$) is set to be higher than the melt pressure, because the surrounding viscous melt prevents the expansion of gas bubbles from being subjected to a sudden depressurization. The pressure difference between the gas bubbles and the

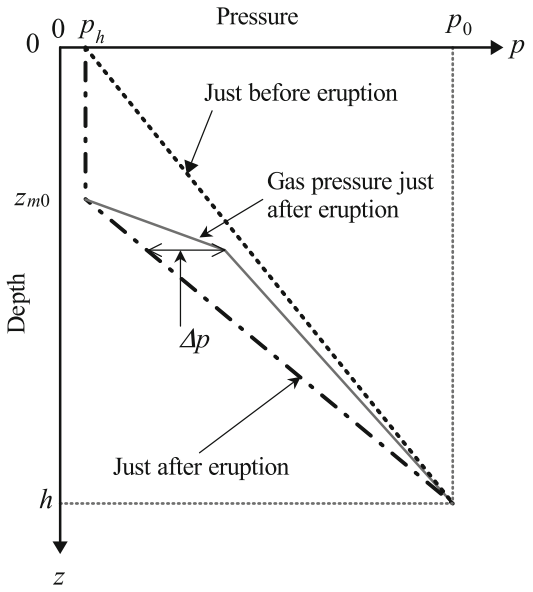

Fig. 3. Depth profiles of pressure just before and after the eruption in the conduit. Dotted lines shows the normal stress added to the conduit wall just before an eruption. Chained line shows the normal stress added to the conduit wall just after an eruption. Solid line shows the pressure of gas phase in bubbles just after eruption.

melt is set to change with depth. In the present study, we set the initial gas pressure as shown in Fig. 3, so that the amount of melt decompression decreases with depth. The initial pressure difference also decreases with depth into the deeper portion of the conduit. The pressure difference at the top of the conduit is set to be zero, and linearly increases with depth at the shallowest part. This is because the top of the magma is subjected to depressurization for a longer time. The pressure difference has a maximum, Δp, at $z = h - 0.9 \times (h - z_{m0})$, where h is the conduit length, and linearly decreases with depth.

The initial magma void ratio is calculated from the initial gas pressure and volatile concentration. We further assume that the dissolved volatile in the melt is at equilibrium just before the eruption. From the mass conservation law of volatiles, the initial radius of the elementary cell and the gas bubble satisfy the following equation:

$$\frac{4}{3}\pi S_0^3 \rho_l c_0 = \frac{4}{3}\pi R^3 \rho_{g0} + \frac{4}{3}\pi \left(S^3 - R^3\right) \rho_l c(p_{g0}). \quad (18)$$

Using the above equation and the relationship between the cell and gas bubble radius, the void ratio, the number density of the gas bubbles, and the initial magma void ratio, are related to each other by:

$$\psi_0(z) = \frac{c_0 - c(p_{g0}(z))}{c_0 - c(p_{g0}(z)) + \frac{p_{g0(z)}}{\rho_l RT}}, \quad (19)$$

where $c(p_{g0}(z))$ is the volatile concentration at the initial gas pressure.

2.5 Normalization of the governing equations

For numerical calculations in the present study, we introduce dimensionless variables and constants that are normalized by the scale units shown in Table 2. The scale units are systematically derived from the base units: the reference melt density ρ_r, the conduit length h, and the degree of viscous drag η_f/a^2. The dimensionless variables and constants are:

$$\rho' = \frac{\rho}{\rho_r},\ z' = \frac{z}{h},\ t' = \left(\frac{\rho_r g a^2}{8\eta_f h}\right) t,$$
$$p' = \frac{p}{\rho_r g h},\ v' = \left(\frac{8\eta_f}{\rho_r g a^2}\right) v. \quad (20)$$

We further introduce three characteristic time-scale parameters: (1) the Poiseuille flow time scale τ_p, which is determined from the size of the conduit and the density and viscosity of the melt; (2) the viscous deformation time scale τ_v, which is determined from the initial pressure difference between the gas bubble and the melt; and (3) the diffusion time scale τ_d, which is determined from the number density of gas bubbles and the diffusion coefficient of the volatile in the melt. These are expressed as (Navon and Lyakhovsky, 1998; Mason *et al.*, 2006):

$$\text{Poiseuille flow time scale} \quad \tau_p = \frac{8\eta_f h}{g\rho_r a^2}, \quad (21a)$$

$$\text{Viscous deformation time scale} \quad \tau_v = \frac{\eta_f}{\Delta p}, \quad (21b)$$

$$\text{Diffusion time scale} \quad \tau_d = \left(n_*^{\frac{2}{3}} D\right)^{-1}. \quad (21c)$$

Table 2. Scale units used in this study.

Physical quantity	Scale unit	Typical value
Density ρ	ρ_r	2500 kg/m^3
Length z	h	1000 m
Time t	$\tau_p = 8\eta_f h/\rho_r g a^2$	320 s
Pressure p	$p_r = \rho_r g h$	25 MPa
Velocity v	$h/\tau_p = \rho_r g a^2/8\eta_f$	3 m/s

The Poiseuille flow time scale represents the time scale of macro-scale magma ascent processes due to pressure gradients in the conduit. The viscous deformation time scale and diffusion time scale represent the time scales of micro-scale gas bubble growth processes. When the Poiseuille flow time scale is smaller than the viscous deformation time scale and the diffusion time scale, the magma ascent velocity is faster than the bubble growth speed so that magma reaches the ground surface until the gas bubbles have grown sufficiently. When the viscous deformation time scale is smaller than the diffusion time scale, the bubble growth process is governed by the viscous resistance of the melt. When the diffusion time scale is smaller than the viscous deformation time scale, the bubble growth process is governed by the diffusive volatile flow from melt to gas bubbles. These characteristic time-scale parameters have often been used in previous magma flow models, although the coefficients on the normalized parameters are sometimes different (Lensky *et al.*, 2004).

Then, we obtain the dimensionless equations:

$$\frac{\partial \rho'}{\partial t'} = -\frac{\partial}{\partial z'}\left(\rho' v'\right), \quad (22)$$

$$\frac{\partial \rho'_e}{\partial t'} = -\frac{\partial}{\partial z'}\left(\rho'_e v'\right) + \frac{\tau_p}{\tau_d} J', \quad (23)$$

$$\frac{\partial \psi}{\partial t'} = -v'\frac{\partial \psi}{\partial z'} + \frac{3}{4}\frac{\tau_p}{\tau_v}\frac{p'_g - p'}{\Delta p'}\left(\frac{\psi}{1-\psi}\right), \quad (24)$$

$$v' = -\left(\frac{\partial p'}{\partial z'} + 1\right), \quad (25)$$

$$J' = 4\left(6\pi^2\right)^{\frac{1}{3}} \rho'_l \cdot \frac{\left(\psi^3 + \psi - 2\psi^2\right)^{\frac{1}{3}}\left((1-\psi)(c_0 - c(R_g)) - \psi\frac{\rho'_e}{\rho'_l}\right)}{2 + \psi - 3\psi^{\frac{1}{3}}}. \quad (26)$$

We solve these dimensionless equations by using the finite difference method. For the numerical calculation, the dimensionless coordinate is divided into equally spaced grid points. The number of grid points covering the whole conduit is always set to be 100. The discrete variables at each grid point are calculated as a function of time by integrating the dimensionless differential equations (22)–(24) with the fourth-order Runge-Kutta method. The magma

head depth, which moves upward with time, is not always located at a grid point. The grid point just below the magma head depth is used for the calculation, and the dimensionless variables at the top grid point are determined by linearly interpolating the values at the boundary of the magma head and the values at the grid just beneath the highest grid. The magma head depth is calculated by using the magma velocity at the top grid point, which is determined from Eq. (25). When the magma head reaches the ground surface, the calculation is stopped.

2.6 Calculation of volcanic deformation

We calculate the volcanic deformation caused by the magmatic pressure change in the conduit. Following Bonaccorso and Davis (1999) and Nishimura (2009), we formulate the volcanic deformation due to the normal stress exerted by magma on the conduit wall. We assume that the conduit radius is sufficiently small compared to the distance from the vent to a station. The ground deformations that we observe are deviations from the initial condition of the magma pressure in the conduit just after an eruption. The radial displacement u_r and the vertical displacement u_z, on the flat ground surface of a homogeneous elastic half-space, are obtained by using the analytical solutions of the displacement field by a pressurized open conduit (Bonaccorso and Davis, 1999):

$$u_r(r,t) = a\int_0^\infty b(z,t)\left[\frac{r}{R^3} - \frac{r}{2}\left(\frac{3z^2}{R^5} - \frac{2\nu}{R^3}\right)\right]\mathrm{d}z, \tag{27}$$

$$u_z(r,t) = a\int_0^\infty b(z,t)\left[\frac{z}{R^3} - \frac{z}{2}\left(\frac{3z^2}{R^5} - \frac{2\nu}{R^3}\right)\right]\mathrm{d}z, \tag{28}$$

where

$$b(z,t) = \frac{dp(z,t)}{\mu}a, \tag{29}$$

$$dp(z,t) = p(z,t) - p(z,0), \tag{30}$$

and r is the horizontal distance from the vent to a station on the flat surface, ν is the Poisson's ratio of the surrounding elastic medium, $\mathrm{d}p(z,t)$ is the excess magma pressure from the initial condition ($t = 0$), μ is the rigidity of the surrounding elastic medium, a is the conduit radius, and $R = \sqrt{r^2 + z^2}$ (Fig. 4). Herein, u_z and u_r are positive when the displacements are upward and outward from the vent, respectively. The tilt γ is expressed as:

$$\gamma = -\frac{\partial u_z}{\partial r}, \tag{31}$$

where γ is positive when the ground is lifted up toward the vent.

Magma pressures calculated from the magma flow model are linearly interpolated from the discretized pressure distribution at each grid point, and are substituted into Eqs. (27), (28) and (31) to obtain the radial and vertical displacements and tilt at each time step. Dimensionless variables are used for the calculation of radial and vertical displacements that are scaled by the conduit length h:

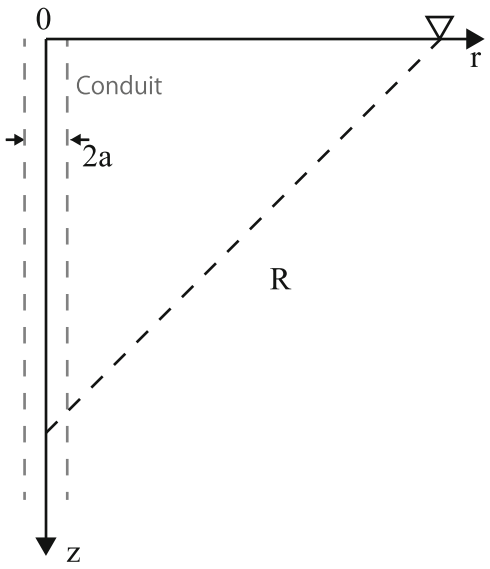

Fig. 4. Coordinate system for the calculation of volcanic deformation.

$$u_r' = \frac{u_r}{h}\ ,\ u_z' = \frac{u_z}{h}. \tag{32}$$

In the following sections, the calculation results are shown using these dimensionless displacements.

3. Simulation Results

3.1 Model parameters

We examine the magma ascent processes in an open conduit and the temporal changes of volcanic deformation for seven model parameters: the pressure at the bottom and top of the conduit (p_0 and p_h), the initial magma head depth (z_{m0}), the pressure difference between gas bubble and melt (Δp), the volatile concentration (c_0) and the ratios of characteristic time scales (τ_p/τ_d and τ_p/τ_v) which appear in the dimensionless equations. In consideration of our assumption that the relative velocities between the gas bubbles and the melt is negligibly small, we use the physical parameters shown in Table 3, in which their typical values and variation ranges are given. The characteristic time scales, τ_p, τ_v and τ_d, are estimated to be 320 s, 1 s and 0.1 s, respectively, for the typical values shown in Table 3. We assume $\mu = 10$ GPa and $\nu = 0.25$ for the surrounding elastic medium.

3.2 General characteristics of magma ascent and volcano deformation

First, we examine the basic behaviors of magma ascent and volcanic deformation for the typical model parameters shown in Table 3. Figure 5 shows the spatio-temporal distributions of melt pressure (a), void ratio (b), and volatile concentration in the melt (c), in the conduit. The variables used in each figure are in dimensionless form. As the magma ascends in the conduit, the melt pressure at all depths increases with time. The amount of the pressure increase is a maximum at the initial magma head depth in the conduit. The maximum pressure change is set to be 4 MPa as a typ-

Table 3. Typical values and variations of magma properties and conduit sizes used in this study.

Property	Symbol	Typical value	Variation range
Melt density	ρ_r	2.5×10^3 kg m^{-3}	
Bulk modulus of melt	K_l	1.2×10^{10} Pa	
Gas constant	B	8.31 J K^{-1} mol^{-1}	
Magma temperature	T	1100 K	
Melt viscosity	η_f	10^5 Pa s	10^4–10^5 Pa s
Gas bubble number density	n	10^{15} m^{-3}	10^{12}–10^{18} m^{-3}
Diffusivity	D	10^{-9} m^2/s	10^{-10}–10^{-8} m^2/s
Initial pressure difference	Δp	0.1 MPa	0.1–1 MPa
Conduit radius	a	10 m	3–10 m

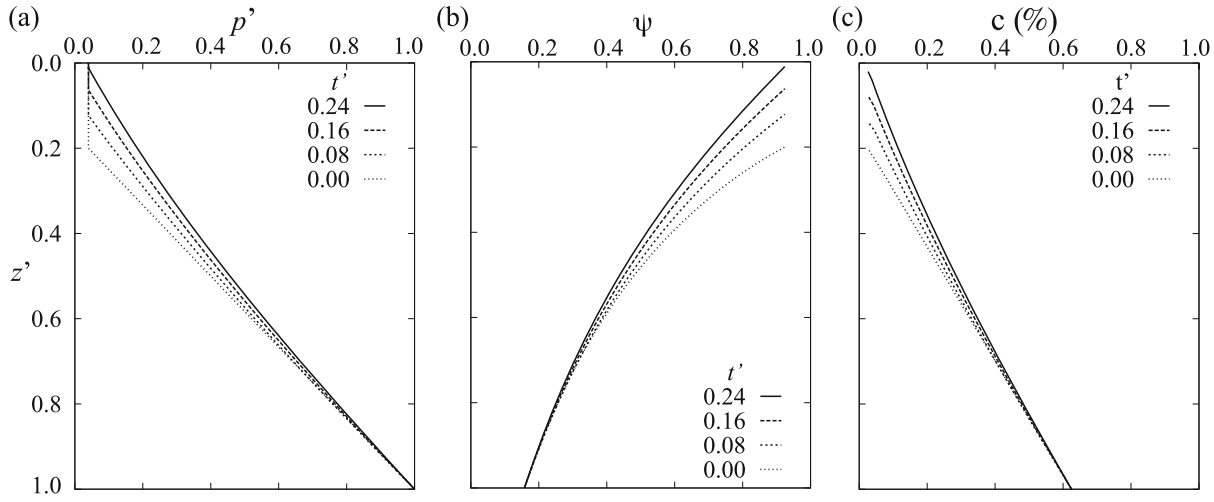

Fig. 5. Temporal changes of the depth variation of (a) the void ratio ψ, (b) the melt pressure p' in the conduit and (c) the volatile concentration in melt c.

ical model parameter. At the shallow part of the conduit, many volatiles in the melt exsolve to gas bubbles. As a result, the void ratio becomes large and the volatile concentration becomes small. The magma ascent rate in the upper part of the conduit is larger than that in the lower part. This is because, in the upper part of the conduit, bulk magma density becomes small due to a large void ratio and gas bubbles largely expand due to a low magma pressure.

Figure 6 shows the spatio-temporal distribution of volcanic deformation caused by magma ascent. The radial and vertical displacements, and the distance from the vent, are expressed by dimensionless forms that are scaled by the conduit length h. The displacements, as well as tilts, increase with the distance r', reach peaks at $r' = 0.1$–0.4, and gradually decrease with distance. As the magma head ascends in the conduit from $t' = 0$ to $t' = 0.24$, the amplitudes of the displacements and tilts increase, and the peaks of the displacements and tilts appear at distances close to the vent. The locations where the tilts show peak values are farther away than those of displacements. These results suggest that the spatio-temporal distribution of volcanic deformation may be used to estimate the depth of the magma head and its temporal changes. Figure 7 shows the temporal changes of volcanic deformation at stations located at different distances from the vent. The figure shows that the deformation rates at locations close to the vent ($r' < 1$) greatly increase with time, despite an almost constant magma ascent speed. This is because the displacements and tilts at a station close to the vent are more affected by the depth change of the magma head in the conduit. For example, a tilt at $r' = 0.2$ shows a downlift toward the vent after the start of magma ascent, and then changes to an uplift. Whereas the deformation rates at larger distances ($r' \geq 1$) change little with time. Thus, the displacements and tilts at a station far from the vent increase, being proportional to the magma head depth.

3.3 Effects of the model parameters

To examine the effects of the model parameters on the deformation, we simulate the magma ascent by changing one parameter and fixing the others. The temporal changes of the volcanic deformation at $r' = 1.0$ are examined to omit the effect of depth change of the magma head.

Figure 8 shows the temporal changes in radial displacements and tilts for different magma pressures at the bottom of the conduit, p'_0. The figures are plotted in a logarithmic scale to observe the differences in the deformation rate. The magnitude of p'_0 can be related to the magma pressure at the bottom of the conduit: $p'_0 = 1.0$ represents the case in which the magma pressure at the bottom of the conduit is equal to the lithostatic pressure of the surrounding rock. The latter case may occur when the density of the magma is smaller than that of the surrounding rocks, which is predicted for a magma with gas bubbles. It is found that the radial displacement and tilt change for a large p'_0 (=1.0) is almost proportional to time. This constant rate is analogous to a prediction from the no-gas growth model

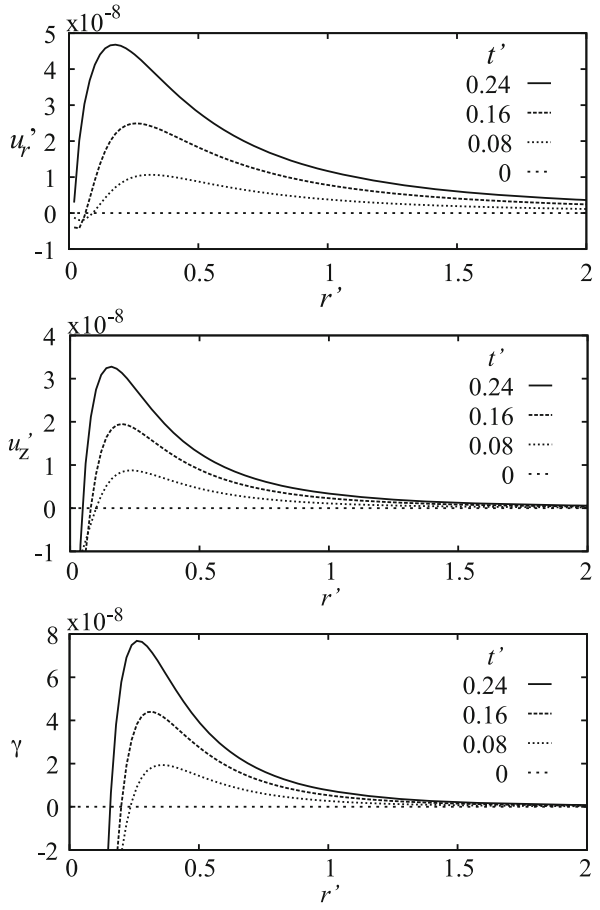

Fig. 6. Spatial variations of radial and vertical displacements u_r' and u_z' and tilts γ for different lapse times measured from the time just after the eruption ($t' = 0$). All variables are scaled by the conduit length (h).

in Nishimura (2009). That is, the magma ascent process is more affected by the pressure gradient than by volume expansion due to gas bubble growth. On the other hand, for a small p_0' (= 0.6), the displacement and tilt changes increase with time, being proportional to $t'^{1.5}$. This accelerated change is the same as that predicted by the diffusive gas bubble growth model of Nishimura (2009). This indicates that a decreasing p_0' decreases the pressure gradient, so that a volume expansion due to the gas bubble growth process becomes the dominant driving force. These results suggest that the rate of volcanic deformation is affected by the initial pressure gradient built up in the conduit just after eruption.

Figure 9 shows the temporal changes in the radial displacement at $r' = 1.0$ for different time-scale ratios, τ_p/τ_v and τ_p/τ_d. In the range of the model parameters shown in Table 3, τ_v and τ_d are always smaller than τ_p. This condition represents a bubble growth process that proceeds faster than the Poiseuille magma flow. When $p_0' = 1.0$ (Figs. 9(a, b)), the characteristic time-scale parameters do not affect the temporal changes in the deformation because the effect of the pressure gradient in the conduit is large enough to decrease the effect of gas bubble growth. When $p_0' = 0.6$ (Figs. 9(c, d)), the radial displacements increase with time, being proportional to $t'^{1.5}$ in the range of the model parameters shown in the Table 3 (τ_p/τ_v = 320–1280). These results are the same as those shown in Fig. 8. For the case of a smaller value ($\tau_p/\tau_v = 0.1$), the radial displacement linearly increases with time. The small τ_p represents the condition where the conduit radius is sufficiently large and/or magma viscosity is low. In this case, a small viscous resistance in the Poiseuille flow results in magma moving upward before gas bubble growth, which decreases the effect of the driving force by the volume expansion of the gas bubbles. A difference in τ_p/τ_d, does not change temporal changes in the deformation, even for $p_0' = 0.6$. We use the analytical solution of the diffusive mass flux of volatiles for the bubble growth process, assuming that the diffusion of volatiles in the melt is fast. Therefore, to investigate the effect of diffusion time-scales in detail, it is necessary to solve the diffusion equation accurately. These simulations indicate that the time scale parameter τ_p/τ_v affects the temporal changes of deformation when the pressure gradient in the conduit is small.

Figure 10 compares the temporal changes in the radial displacement and tilt at $r' = 1.0$ for a magma with, and without, volatiles. When the magma has no volatiles ($c_0 = 0.0\%$), the driving force of the magma is just the pressure gradient in the conduit. In this case, as the magma ascends, the ascent velocity decreases with time and becomes almost zero near the ground surface, since the pressure gradient in the magma approaches that caused by the gravitational force. As a result, the time rates of the radial displacement and tilt decrease with time. On the other hand, the radial displacement and tilt almost constantly increase with time when the magma includes volatiles ($c_0 = 1.0\%$). This is because the magma pressure gradient in the conduit is small due to a low magma density and does not change much with time. In addition, the driving force for the magma with volatiles include the pressure gradient in the conduit and the volume expansion due to gas bubble growth. Therefore, the rate of volcanic deformation does not decrease as does the magma without volatiles. The amplitudes of volcanic deformation due to magma without volatiles are larger than those when the magma contains gas bubbles, when the magma reaches the ground surface because the magma density is large.

Figure 11(a) compares the temporal changes in the radial displacements at $r' = 1.0$ for different initial pressure differences between the gas bubbles and the melt $\Delta p'$. The parameter $\Delta p'$ changes from 0.004 to 0.04, which corresponds to a pressure of 0.1–1.0 MPa. Since $\Delta p'$ increases the initial volatile supersaturation in the melt, the mass flux of volatiles from the saturated melt to the gas bubbles for large $\Delta p'$ is faster at the beginning of the magma ascent than that for small $\Delta p'$. This is recognized in the differences of the power of the lapse time of the temporal changes in the radial displacement, while the magma ascending time and the final amplitudes of the deformation are little affected by $\Delta p'$. Figure 11(b) shows the temporal changes in the radial displacements for magma pressure at the top of the conduit p_h', which may be related to the weight or viscous resistance of cap rocks. The large magma head pressure hinders the magma ascent; hence, the amplitude of the volcanic deformation decreases with increasing p_h'. The magma head pressure does not affect the magma ascent process as much

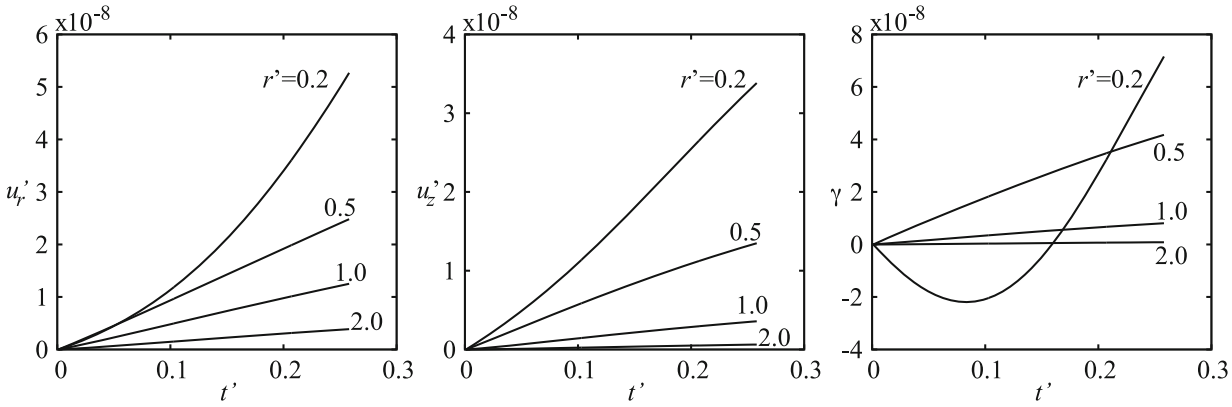

Fig. 7. Temporal changes of radial and vertical displacements and tilt at different horizontal distances from the vent.

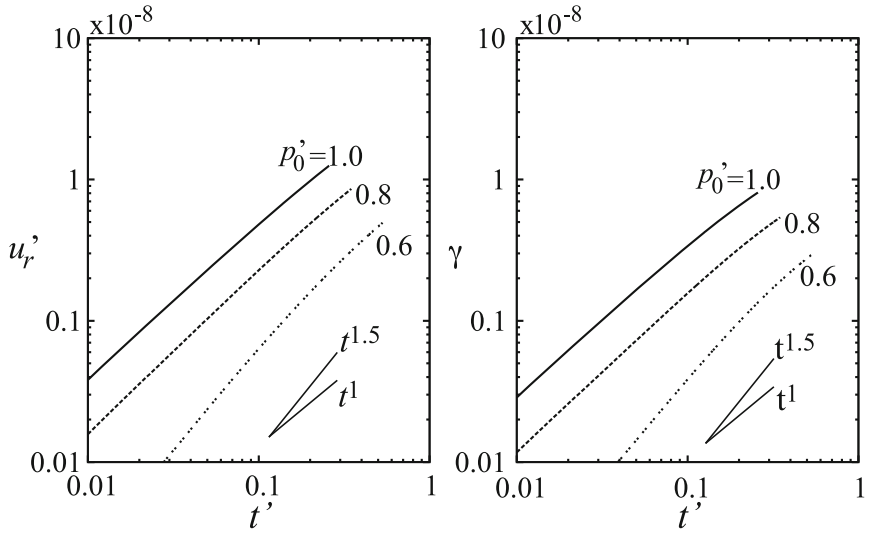

Fig. 8. Temporal changes of radial displacements and tilts for different magma pressure at the bottom of the conduit p_0' at $r' = 1.0$.

as does the pressure p_0' at the bottom of the conduit. Figure 11(c) shows the temporal changes in the radial displacements for different initial magma head depths z_{m0}', which may be related to the volume of volcanic products from a previous eruption. As z_{m0}' increases, the magma ascending time to reach the ground surface becomes longer and the amplitudes of the displacement increase. z_{m0}' has little effect on the rate of volcanic deformation.

4. Discussion

We have presented a magma ascent model in an open conduit and examined the basic behavior of volcanic deformations for various model parameters. First, we examine whether or not our model can explain the geodetic and seismic data observed at active volcanoes. Interval times of eruptions and tilt amplitudes observed at the Semeru volcano, Indonesia, are about 3 to 30 minutes, and about 1–10 nanoradian at a distance of 500 m away from the active vent (figure 5 of Iguchi *et al*., 2008). At the Suwanose-jima volcano, Japan, uplifts start about 120 s before explosions and about 30×10^{-6} m vertical uplifts are observed at a distance of 500 m (station SWC-UD, in Iguchi *et al*., 2008, Fig. 4). These volcanoes erupt basaltic-andesitic magma which has a viscosity of about 10^4–10^5 Pa s. Also, an analysis of the explosion earthquakes uses a conduit radius of 10 m (Nishimura, 1998), but recent activities of Suwanose-jima are small, so we assume a conduit radius, a, of 5 m. The eruption size of the Semeru volcano is also similar to that of Suwanose-jima. Tameguri *et al*. (2004) determined the initial phase of the explosion earthquakes at about 500 m, so we tentatively set the conduit length to be 1000 m. The pressure at the bottom, p_0, is set to be 20 MPa, which is obtained from the magma static pressure at that depth. Thus, using typical model parameters of the magma properties shown in Table 3, we estimate the magma ascent time to be 13.5 minutes and the maximum amplitude of tilt to be 3 nanoradian at $r = 500$ m for $c_0 = 0.5\%$. Also, assuming $z_{m0} = 400$ m, and $\eta_f = 8 \times 10^4$ Pa s, the duration time of the magma ascent and the vertical displacement are estimated to be 120 s and 30×10^{-6} m, respectively, at $r = 500$ m. These estimated values are reasonably matched with the observations. However, as indicated in Eqs. (27) and (28), the amplitude of deformation is proportional to the square of the conduit radius and increases with the conduit length. Also, the magma ascending time depends on the Poiseuille flow time, τ_p, that is mainly affected by con-

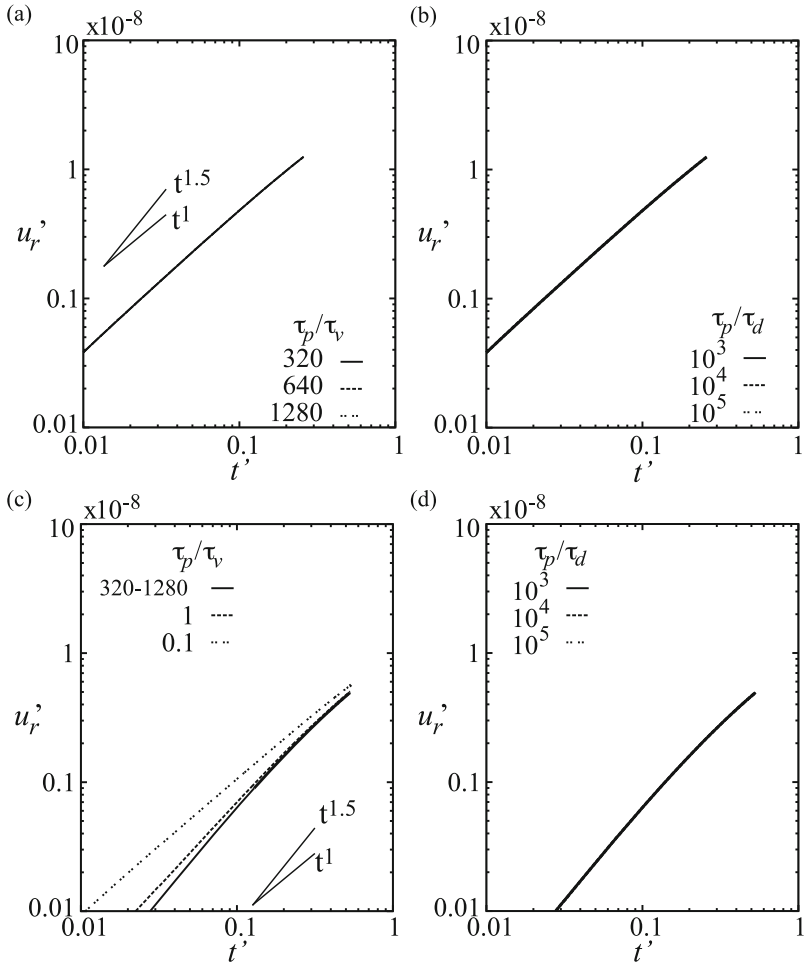

Fig. 9. Temporal changes of radial displacements for different ratios of the Poiseuille flow time scale to the viscous deformation time scale τ_p/τ_v (a), (c) and the ratios of Poiseuille flow time scale to the diffusion time scale τ_p/τ_d (b), (d) at $r' = 1.0$, as plotted on logarithmic scales. (a) and (b) for $p_0' = 1.0$. (c) and (d) for $p_0' = 0.6$. All lines in Fig (a), (b) and (d) are overlapped.

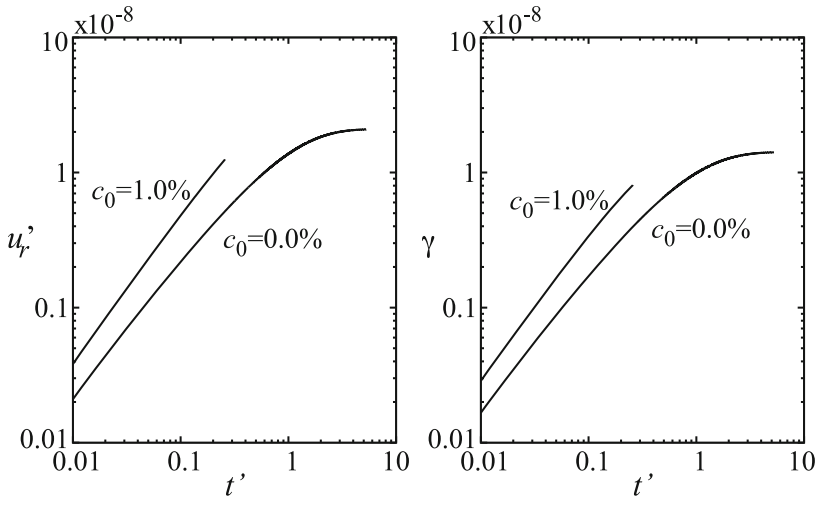

Fig. 10. Comparison of temporal changes of radial displacement and tilt for the magma with gas bubbles ($c_0 = 1.0\%$) and that without gas bubbles ($c_0 = 0.0\%$) at $r' = 1.0$.

duit radius, magma viscosity and the length of the conduit. We may be able to assume a reasonable conduit length for the volcanic eruptions, where dense geodetic observation data are available, and determine the viscosity by analyzing the volcanic samples. Such data enable us to discuss in more detail the magma ascent process of a volcanic eruption by carrying out these kinds of observation. Also, considering the characteristics of temporal changes of volcano deformation, such as acceleration or non-acceleration, we may further discuss the magma ascent processes at active

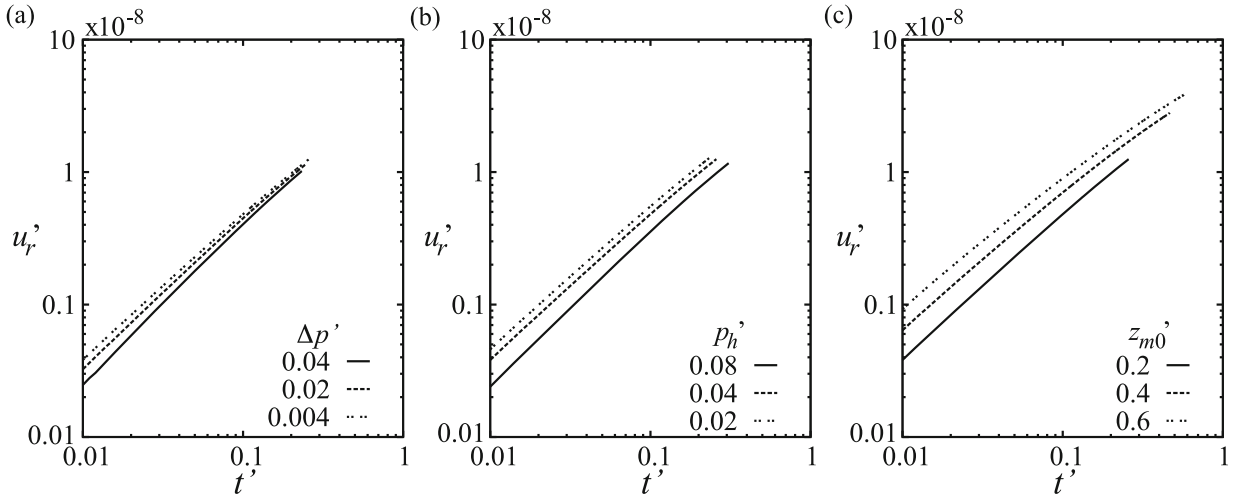

Fig. 11. Temporal changes of radial displacements at $r' = 1.0$ for the model parameters. (a) Initial pressure difference between a gas bubble and melt $\Delta p'$, (b) magma pressure at the top of the conduit p'_h, and (c) the initial magma head depth z'_{m0} in the conduit.

volcanoes and estimate the physical magma parameters.

Our model has simplified the magma process in the conduit by using mathematical representations for bubble growth and fluid motions that are often used in previous studies. The model mainly includes the main driving forces of magma ascent: the volume expansions of gas bubbles and the pressure gradient in the fluid. However, we did not consider, for example, out-gassing from the magma in the conduit (Ida, 2007), or fragmentations of the magma (e.g., Melnik, 2000; Koyaguchi *et al.*, 2008), because these processes are complex and are still under investigation. Also, several studies based on geophysical observation data present a model consisting of a gas pocket at a very shallow depth just beneath a lava dome, or cap rocks, for Vulcanian eruptions (e.g., Ishihara, 1990). These processes require to be modeled to further examine various kinds of volcano inflations at active volcanoes. We have calculated the volcano deformation assuming that the displacements of the conduit wall due to magma pressure is much smaller than the conduit radius. But, when the conduit is like a thin dike, it is necessary to include the interaction of magma flow and conduit deformation. In addition, finite element methods, or boundary element methods, are useful for calculating the deformation of volcanoes with a steep topography.

5. Conclusion

We have numerically simulated magma ascents in an open conduit, using a two-phase one-dimensional magma flow model to examine the bubble growth in magma with a volcanic deformation that can be recorded captured by geodetic measurement. The main results are summarized as follows:

(1) The magma pressure at the bottom of the conduit strongly affects the rate of the temporal changes in volcanic deformation. When the pressure at the bottom of the conduit is small, the pressure gradient decreases, and the volume expansion due to the gas bubble growth becomes dominant in the magma ascent process. As a result, the displacements and tilt increase, are proportional to the 1.5th power of time. On the other hand, when the pressure at the bottom of the conduit is large, the displacements and tilt increase linearly proportional to the lapse time. This is probably because the magma ascent process is dominated by the magmatic pressure gradient in the conduit.

(2) The ratio of the characteristic time-scale parameter (τ_p/τ_v) affects the temporal changes of volcanic deformation, when the pressure gradient of the magma in the conduit is small. When $\tau_p/\tau_v < 1$, the effect of gas bubble growth processes decreases due to the viscous resistance of the melt, and displacements and tilt increase and are proportional to the lapse time.

(3) When volatiles are not included in the magma, the magma ascent velocity decreases with time and the deformation decelerates, since the driving force, which is the pressure gradient, becomes weak with the magma ascent.

(4) The initial conditions regarding the pressure difference between the gas bubble and the melt, and the magma head depth, change the magma ascent time and the amplitude of the volcanic deformation with little affect on the time rate of displacements and tilt.

Acknowledgments. Careful comments from an anonymous reviewer and Phil Dawson improved this manuscript. We appreciate Nobuo Geshi for editorial efforts. This study is supported by the Ministry of Education, Culture, Sports, Science and Technology (MEXT) of Japan (No. 21540427). R. Kawaguchi was partly supported by the International Advanced Research and the Education Organization (IAREO) and Global COE program of Tohoku University.

References

Anderson, K. and P. Segall, Physics based models of ground deformation and extrusion rate at effusively erupting volcanoes, *J. Geophys. Res.*, **116**, B07204, doi:10.1029/2010JB007939, 2011.

Arefmanesh, A. and S. G. Advani, Diffusion-induced growth of a gas bubble in a viscoelastic fluid, *Rheol. Acta*, **30**, 274–283, 1991.

Barmin, A., O. Melnik, and R. S. J. Sparks, Periodic behavior in lava dome eruptions, *Earth Planet. Sci. Lett.*, **199**, 173–184, 2002.

Bonaccorso, A. and P. M. Davis, Models of ground deformation from vertical volcanic conduits with application to eruptions of Mount St. Helens and Mount Etna, *J. Volcanol. Geotherm. Res.*, **104**, 10,531–10,542, 1999.

Chouet, B., P. Dawson, and M. Nakano, Dynamics of diffusive bubble growth and pressure recovery in bubbly rhyolitic melt embedded in an elastic solid, *J. Geophys. Res.*, **111**, B07310, doi:10.1029/2005JB004174, 2006.

Costa, A., O. Melnik, and R. S. J. Spaeks, Controls of conduit geometry and wallrock elasticity on lava dome eruptions, *Earth Planet. Sci. Lett.*, **260**(1–2), 137–151, doi:10.1016/j.epsl.2007.05.024, 2007.

Davis, P. M., Surface deformation due to inflation of an arbitrarily oriented triaxial ellipsoidal cavity in an elastic half-space, with reference to Kilauea Volcano, Hawaii, *J. Geophys. Res.*, **91**, 7429–7438, 1986.

De Michieli Vitturi, M., A. B. Clarke, A. Neri, and B. Voight, Effects of conduit geometry on magma ascent dynamics in dome-forming eruptions, *Earth Planet. Sci. Lett.*, **272**(3–4), 567–578, doi:10.1016/j.epsl.2008.05.025, 2008.

Ida, Y., Driving force of lateral permeable gas flow in magma and the criterion of explosive and effusive eruptions, *J. Volcanol. Geotherm. Res.*, **162**(3–4), 172–184, doi:10.1016/j.jvolgeores.2007.03.005, 2007.

Iguchi, M., H. Yakiwara, T. Tameguri, M. Hendrasto, and J. Hirabayashi, Mechanism of explosive eruption revealed by geophysical observations at the Sakurajima, Suwanosejima and Semeru volcanoes, *J. Volcanol. Geotherm. Res.*, **178**(1), 1–9, doi:10.1016/j.jvolgeores.2007.10.010, 2008.

Ishihara, K., Pressure source and induced ground deformation associated with explosive eruptions at an andesitic volcano: Sakurajima volcano, Japan, in *Magma Transport and Storage*, edited by Ryan, M. P., 335–356, John Wiley & Sons, 1990.

Koyaguchi, T., B Scheu, N. Mitani, and O. Melnik, A fragmentation criterion for highly viscous bubbly magmas estimated from shock tube experiments, *J. Volcanol. Geotherm. Res.*, **178**(1), 58–71, doi:10.1016/j.jvolgeores.2008.02.008, 2008.

Lensky, N. G., O. Navon, and V. Lyakhovsky, Bubble growth during decompression of magma: experimental and theoretical investigation, *J. Volcanol. Geotherm. Res.*, **129**(1–3), 7–22, doi:10.1016/S0377-0273(03)00229-4, 2004.

Lyakhovsky, V., S. Hurwitz, and O. Navon, Bubble growth in rhyolitic melts: experimental and numerical investigation, *Bull. Volcanol.*, **58**, 19–32, 1996.

Mason, R., A. Starostin, O. Melnik, and R. S. J. Sparks, From Vulcanian explosions to sustained explosive eruptions: The role of diffusive mass transfer in conduit flow dynamics, *J. Volcanol. Geotherm. Res.*, **153**(1–2), 148–165, doi:10.1016/j.jvolgeores.2005.08.011, 2006.

Melnik, O., Dynamics of two-phase conduit flow of high-viscosity gas-saturated magma: large variations of sustained explosive eruption intensity, *Bull. Volcanol.*, **62**, 153–170, 2000.

Melnik, O. and R. S. J. Sparks, Modelling of conduit flow dynamics during explosive activity at Soufriere Hills Volcano, Monserrat, in *The eruption of Soufriere Hills Volcano, Monserrat, from 1995 to 1999*, edited by Druitt, T. H. and Kokelaar, B. P., Memoirs of Geol. Soc., London, 307–317, 2002.

Mogi, K., Relations between the eruptions of various volcanoes and the deformations of the ground surface around them, *Bull. Earthq. Res. Inst. Univ. Tokyo*, **36**, 99–134, 1958.

Nakanishi, M. and T. Koyaguchi, A stability analysis of a conduit flow model for lava dome eruptions, *J. Volcanol. Geotherm. Res.*, **178**, 46–57, doi:10.1016/j.jvolgeores.2008.01.011, 2008.

Navon, O. and V. Lyakhovsky, Vesiculation process in silicic magmas, in *Physics of Explosive Eruption*, edited by Gilbert, G. S. and Sparks, R. S. J., Geological Society of London, 27–50, 1998.

Nishi, K., M. Hendrasto, I. Mulyana, U. Rosadi, and M. A. Purbawinata, Micro-tilt changes preceding summit explosions at Semeru volcano, Indonesia, *Earth Planets Space*, **59**, 151–156, 2007.

Nishimura, T., Source mechanisms of volcanic explosion earthquakes: single force and implosive sources, *J. Volcanol. Geotherm. Res.*, **86**, 97–106, 1998.

Nishimura, T., Pressure recovery in magma due to bubble growth, *Geophys. Res. Lett.,*, **31**, L12613, doi:10.1029/2004GL019810, 2004.

Nishimura, T., Ground deformation due to magma ascent with and without degassing, *Geophys. Res. Lett.,* **33**, L23309, doi:10.1029/2006GL028101, 2006.

Nishimura, T., Ground deformation caused by magma ascent in an open conduit, *J. Volcanol. Geotherm. Res.*, **187**(3–4), 178–192, doi:10.1016/j.jvolgeores.2009.09.001, 2009.

Nishimura, T., M. Iguchi, R. Kawaguchi, Surono, M. Hendrasto, and U. Rosadi, Inflations prior to Vulcanian eruptions and gas bursts detected by tilt observations at Semeru Volcano, Indonesia, *Bull. Volcanol.*, **74**, 903–911, 2012.

Okada, Y., Surface deformation due to shear and tensile faults in a half-space, *Bull. Seismol. Soc. Am.*, **75**, 1135–1154, 1985.

Okumura, S., M. Nakamura, A. Tsuchiyama, T. Nakano, and K. Uesugi, Evolution of bubble microstructure in sheared rhyolite: Formation of a channel-like bubble network, *J. Geophys. Res.*, **113**(B7), B07208, doi:10.1029/2007JB005362, 2008.

Proussevitch, A. A. and D. L. Sahagian, Dynamics of coupled diffusive and decompressive bubble growth in magmatic systems, *J. Geophys. Res.*, **101**, 17,447–17,517, 1996.

Proussevitch, A. A., D. L. Sahagian, and A. T. Anderson, Dynamics of diffusive bubble growth in magmas: isothermal case, *J. Geophys. Res.*, **98**, 283–307, 1993.

Ripepe, M. and A. J. L. Harris, Dynamics of the 5 April 2003 explosive paroxysm observed at Stromboli by near-vent thermal, seismic and inflasonic array, *Geophys. Res. Lett.*, **35**, L07306, doi:10.1029/2007GL032533, 2008.

Scriven, L. E., On the dynamics of phase growth, *Chem. Eng. Sci.*, **10**, 1–13, 1959.

Shimomura, Y., T. Nishimura, and H. Sato, Bubble growth processes in magma surrounded by elastic medium, *J. Volcanol. Geotherm. Res.*, **155**, 307–322, doi:10.1016/j.jvolgeores.2006.04.003, 2006.

Sparks, R. S. J., The dynamics of bubble formation and growth in magmas: a review and analysis, *J. Volcanol. Geotherm. Res.*, **3**, 1–37, 1978.

Tameguri, T., M. Iguchi, and H. Yakiwara, Analysis of eruption earthquakes accompanied with small-scale eruptions at Suwanosejima volcano in November, 2003, *Ann. Disast. Prev. Inst., Kyoto Univ.*, **47 B**, 773–777, 2004 (in Japanese with English abstract).

Voight, B., A. T. Linde, I. S. Sacks, G. S. Mattioli, R. S. J. Sparks, D. Elsworth, D. Hidayat, P. E. Malin, E. Shalev, C. Widiwijayanti, S. R. Young, V. Bass, A. Clarke, P. Dunkley, W. Johnston, N. McWhorter, J. Neuberg, and P. Williams, Unprecedented pressure increase in deep magma reservoir triggered by lava-dome collapse, *Geophys. Res. Lett.*, **33**(3), L03312, doi:10.1029/2005GL024870, 2006.

Wilson, L., R. S. J. Sparks, and G. P. L. Walker, Explosive volcanic eruption-IV. The control of magma properties and conduit geometry on eruption columm behaviour, *Geophys. J. R. Astron. Soc.*, **63**, 117–148, 1980.

Woods, A. W. and T. Koyaguchi, Transitions between explosive and effusive eruptions of silicic magmas, *Nature*, **370**, 641–644, 1994.

Yoshida, S. and T. Koyaguchi, A new regime of volcanic eruption due to the relative motion between liquid and gas, *J. Volcanol. Geotherm. Res.*, **89**, 303–315, 1999.

R. Kawaguchi (e-mail: kawaguchi@zisin.gp.tohoku.ac.jp), T. Nishimura, and H. Sato